ACS APPLIED MATERIALS & INTERFACES

Research Article

www.acsami.org

PbS Quantum Dots Capped with Amorphous ZnS for Bulk Heterojunction Solar Cells: The Solvent Effect

Lidong Sun and Qing Wang*

Department of Materials Science and Engineering, Faculty of Engineering, NUSNNI-NanoCore, National University of Singapore, Singapore 117576

Supporting Information

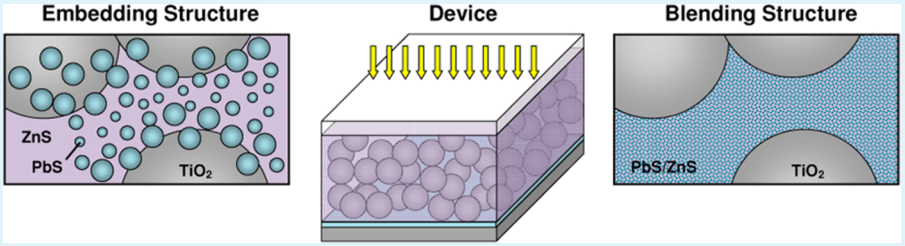

ABSTRACT: In this study, two distinct structures of PbS quantum dots (QDs) are produced with amorphous ZnS as the capping material by successive ionic layer adsorption and reaction. With methanolic solution, spherical PbS QDs (~5 nm) are embedded in the ZnS matrix (i.e., embedding structure), exhibiting relatively large distance between the QDs. With aqueous solution, irregularly shaped PbS QDs (<3 nm) blend intimately with the ZnS medium (i.e., blending structure), showing indiscernible QD spacing. This is attributed to a relatively low reactivity of Pb^{2+} ions in water, suppressing quantum dot growth in the mesopores. Bulk heterojunction of mesoporous TiO_2 substrate filled up with the blending configuration shows superior photovoltaic performance to the embedding architecture, because of the small QD size and close distance between the QDs.

KEYWORDS: *quantum dots, solar cells, bulk heterojunction, PbS, ZnS*

INTRODUCTION

Development of third-generation photovoltaics aims to surpass the Shockley-Queisser limit at low cost.[1] Quantum dot (QD) solar cell is such a promising alternative with limiting conversion efficiency of ~44% by making full use of multiple exciton generation (MEG).[2,3] Photovoltaic devices based on colloidal QD arrays have been studied intensively, which exhibit impressive photocurrent and show great potential to achieve high efficiency with the MEG effect.[4−6] Two major device configurations prevail nowadays with the QD arrays, that is, Schottky junction[7−9] and heterojunction.[6,10−13] In both architectures, only two-dimensional planar junctions are created by forming compact QD layers on top of the substrates,[6−13] even mesoporous substrates are used.[12,13] To further advance charge separation and collection, researchers explored three-dimensional bulk heterojunctions by incorporating the QDs into substrates of large pores, e.g., electrodes comprising very large TiO_2 particles (150−250 nm),[14] TiO_2 nanopillars with oriented macroporous open structures (nanopillar spacing 275 nm),[15] or TiO_2 nanowire networks (interbundle separation ~300 nm).[16] It is noteworthy that such bulk heterojunctions can be achieved only with substrates having large pores, in view of the bulky nature of the colloidal QDs, despite more efficient charge collection being expected with mesoporous substrates.

In our previous work,[17] a unique bulk heterojunction based on mesoporous TiO_2 film was produced, which was filled up with PbS QDs embedded in ZnS matrix. The bulk heterojunction was constructed with an in situ approach (i.e., successive ionic layer adsorption and reaction, or SILAR) as opposed to the ex situ method widely used in colloidal QDs. Inorganic ZnS was employed to confine the PbS QDs, considering (1) type I heterojunction is formed at PbS/ZnS interfaces, rendering a quantum-well like structure; (2) ZnS can hardly form any solid solution with PbS at room temperature; (3) both ZnS and PbS are accessible with SILAR method. In this scenario, the PbS QDs are physically separated by the ZnS, making the photogenerated carriers in the QDs confined by the potential barriers from the ZnS and thus reducing the cooling rate of hot carriers while on the other hand promoting the rate of impact ionization. As compared to the planar heterojunction, the bulk counterpart provides a rapid charge separation by drastically shortening electron hopping distance while maintaining strong optical absorption by the quantum dots. This will, in turn, facilitate hole transport and collection processes.[18] Besides, the inorganic ZnS can passivate the surface states of PbS QDs effectively by a bridging sulfur layer, in contrast to the high density of surface states present in conventional colloidal QDs using organic molecules as the capping agents.[19−21] In this regard, the use of ZnS echoes the developing trend of colloidal QDs where inorganic capping ligands instead of organic

Received: June 4, 2014
Accepted: July 29, 2014
Published: July 29, 2014

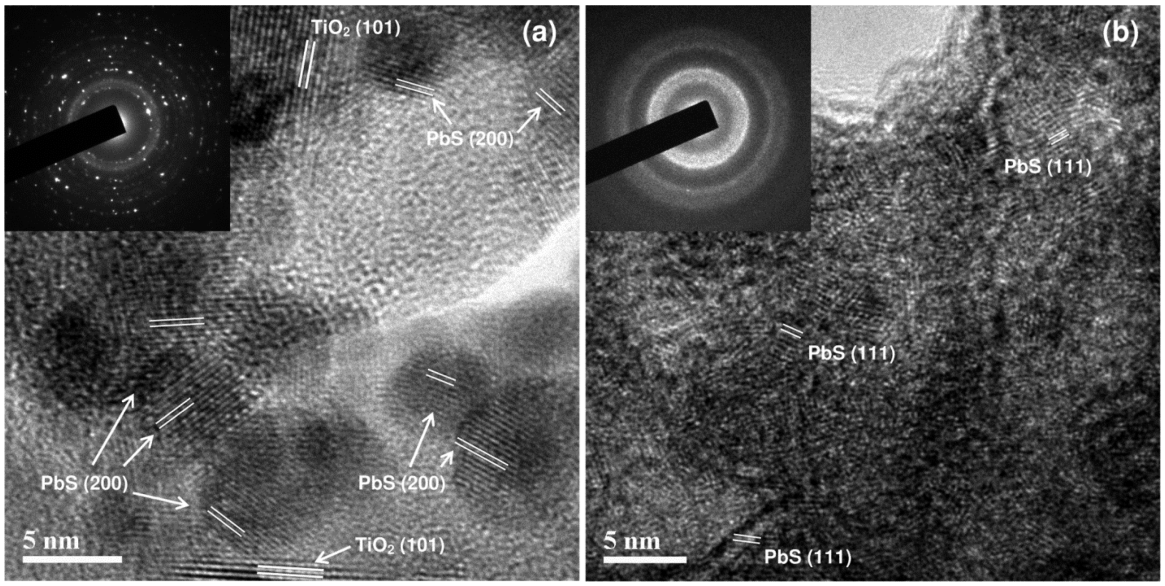

Figure 1. Transmission electron microscopy (TEM) images of PbS quantum dots (a) embedded in and (b) blending with ZnS dielectric matrix prepared in methanolic and aqueous solution, respectively. Insets are corresponding selected area electron diffraction patterns.

molecules have been widely studied. For example, Talapin's group synthesized various quantum dots capped with metal chalcogenide ligands;[22,23] Sargent's group reported photovoltaic devices using PbS QDs capped with monovalent halide anions with a power conversion efficiency up to 6%,[20] and they later pushed the efficiency to 7% by a hybrid passivation scheme;[21] Tsokkou and co-workers recently fabricated PbS QDs capped with arsenic sulfide ligands.[24] However, in our approach, several key features need to be optimized further, one of which is the distance between QDs which affects the charge transport process.

In the bulk heterojunction where PbS QDs are embedded in the ZnS matrix, a quantum-well-like structure is actually produced, with the PbS being the well and the ZnS being the barrier. In such a structure, charge transport is highly dependent on the thickness of the barrier.[25] Large barrier thickness isolates the wells by preventing significant electronic coupling between adjacent wells. Sufficiently thin barrier enables electronic coupling to occur, and therefore electron distribution becomes delocalized. This gives rise to the formation of minibands which facilitate charge transport between wells. The narrower the barrier, the wider the miniband and the higher the carrier mobility. Accordingly, charge transport in the bulk heterojunction can be tuned by altering the distance between neighboring QDs. In conventional colloidal QD solar cells, ligand exchange is widely adopted to reduce the distance,[26,27] for example, replacing the capping ligand of long chains (e.g., oleates) with shorter ones (e.g., amines, thiols),[28,29] whereas in the bulk heterojunctions an intuitive and straightforward way is to reduce the deposition cycle of ZnS to draw the QDs closer. However, this on the other hand leads to an excessive growth of the PbS QDs, since less ZnS amount is inadequate to confine the QD size.[17] In view of this, it is desirable to seek for other alternative methods.

Within this context, under the same conditions but with different solvents for PbS deposition, two distinct configurations are developed in this study: embedding and blending structures. In the embedding structure, isolated large PbS QDs (~5 nm, spherical shape) are dispersed in the ZnS matrix with substantial distance between the QDs. In the blending architecture, very tiny PbS QDs (<3 nm, irregular shape) are mixed intimately with the ZnS matrix with indiscernible distance between the QDs. Bulk heterojunction of the blending structure exhibit superior photovoltaic performance, owing to a smaller QD size and closer distance between QDs.

RESULTS AND DISCUSSION

Growth of Bulk Heterojunction. Mesoporous TiO_2 electrodes of ~500 nm in thickness were employed as the substrates in the current work. To form bulk heterojunction, the mesopores were filled up with PbS quantum dots and ZnS dielectric medium by SILAR method. In brief, five cycles of PbS were deposited onto the TiO_2 electrode first, hereafter referred to as PbS(5); and five cycles of ZnS were deposited subsequently, hereafter referred to as ZnS(5). Alternating deposition of the PbS(5) and ZnS(5) was carried out continuously to fill up the mesoporous films and also to form overlayers on top of the bulk heterojunctions, hereafter referred to as [PbS(5)/ZnS(5)]n for depositing n rounds of the PbS(5)/ZnS(5) sequentially.

Two different polar solvents were used to dissolve the ionic sources for PbS deposition: methanol and water, as the solubility of $Pb(NO_3)_2$ is considerably different in these solvents, ca. 0.04 and 1.57 M at 20 °C in methanol and water, respectively. The solubility reflects the interaction between solute and solvent. A larger solubility suggests that the Pb^{2+} ions interact strongly with the water molecules. Under the same concentration of 0.02 M in the current study, the Pb^{2+} ions should be less active in water as compared to methanol. The reactivity difference of Pb^{2+} ions in these two solvents can be estimated by transfer activity coefficient, γ_t (Pb^{2+}, $H_2O \rightarrow$ MeOH), defined as[30]

$$\log \gamma_t(Pb^{2+}, H_2O \rightarrow MeOH) = \frac{\Delta G_t^\circ(Pb^{2+}, H_2O \rightarrow MeOH)}{2.303RT} \quad (1)$$

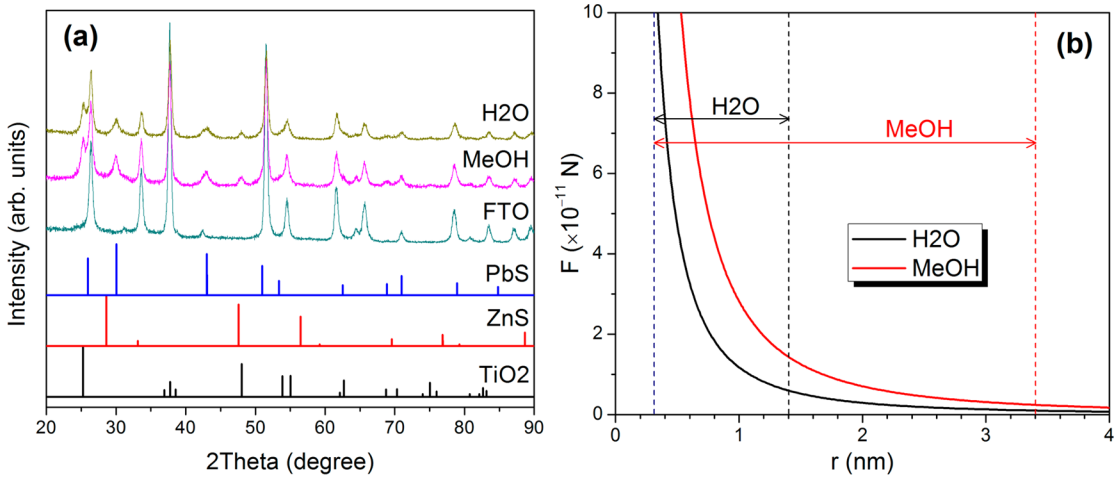

Figure 2. (a) XRD patterns of completely filled bulk heterojunctions prepared using methanol (MeOH) or water (H_2O) as solvent. Data are collected from the corresponding samples shown in Figure S1a, b in the Supporting Information, which are of the same thickness. (b) Electrostatic force as a function of distance between Pb^{2+} and S^{2-} ions in different solvents. The relevant ion association regions are given by dashed lines. Plots are based on calculations with eqs 2 and 3.

where ΔG_t° (Pb^{2+}, $H_2O \rightarrow$ MeOH) is the Gibbs energy of transfer of Pb^{2+} ions from water to methanol, which is about 10.3 kJ/mol at 25 °C,[31] R is the gas constant, T is the absolute temperature. Accordingly, the transfer activity coefficient is calculated to be ~63 at 25 °C, indicating that the reactivity of Pb^{2+} ions in methanol is approximately 63 times that in water. This influences the growth of PbS QDs substantially.

Figure 1 compares the microstructures of the bulk heterojunctions. With methanolic solution, spherical quantum dots of ~5 nm are produced, as shown in Figure 1a. The QDs are assigned to PbS with an interplanar spacing of 2.97 Å, corresponding to the (200) plane of galena phase. Two TiO_2 crystals from the substrate are also visible with an interplanar spacing of 3.52 Å, consistent with the (101) plane of anatase structure. The selected area electron diffraction (SAED) pattern exhibits a typical characteristic of nanocrystalline materials. In contrast, with aqueous solution very tiny quantum dots of irregular shape are developed, as displayed in Figure 1b. The interplanar spacing of these dots is determined to be 3.42 Å, ascribed to the (111) plane of galena PbS. The SAED pattern reveals nearly an amorphous feature while still contains some trace crystal planes, in good agreement with the high-resolution TEM image. In both cases, no crystalline ZnS can be detected. This is in line with the X-ray diffraction (XRD) patterns obtained from the completely filled films, as shown in Figure 2a. Energy-dispersive X-ray spectroscopy (EDS) results exhibit the following compositions through examining the cross sections in Figure S1a, b (see the Supporting Information): Ti:Pb:Zn:S = 1:0.23:0.39:0.74 and 1:0.25:0.51:0.66 (in atomic ratio) for methanol and water, respectively. Apparently both films contain substantial amount of zinc element, which is even higher than that of lead. This suggests that ZnS exists in an amorphous state. As such, the following two configurations can be figured out: spherical PbS quantum dots are embedded in the amorphous ZnS matrix with methanolic solution (i.e., embedding structure), whereas irregular QDs are blended with the amorphous ZnS with aqueous solution (i.e., blending structure). Further indication can be found in Figures S2 and S3 in the Supporting Information. These different constitutions lead to different physical, optical, and photovoltaic properties of the thin films, as will be discussed later.

Formation of the two distinct structures can be related to the reactivity of the Pb^{2+} ions in different solvents. In methanolic solution, the Pb^{2+} ions are so active that it is inclined to grow into large quantum dots. In contrast, the aqueous solution makes the ions less active and thus impedes the growth of QDs, therefore giving rise to much smaller size. However, the content of PbS in both films are comparable according to the EDS results. This indicates that crystal growth is a dominant process in methanolic solution while nucleation is more prevailing in aqueous solution, eventually yielding similar amount of PbS in the mesoporous films. Although the precursor solutions for ZnS growth are the same for both films (aqueous solution), the subsequent deposition of ZnS on PbS is also affected. When water is used as the solvent for PbS deposition, more ZnS are subsequently deposited in the mesopores (cf. EDS results) because of better compatibility (i.e., both are aqueous solutions). On the other hand, the solvent compatibility also facilitates the filling of the mesoporous films. It takes about 3 rounds (n = 3) to fill up the films with aqueous solution while 5 rounds with methanolic solution, as shown in Figure S1 in the Supporting Information.

Consequently, the solvent used is a predominant factor which determines the reactivity of Pb^{2+} ions. The reactivity, in turn, leads to different-sized QDs as well as different distances between the QDs. In addition, previous studies also showed that irregularly shaped PbS QDs were obtained when the size was below 5 nm,[5] whereas spherical QDs were attained with sizes between 5 and 10 nm.[5,32] This is consistent with the results in the present study.

As both heterojunctions comprise comparable amount of PbS QDs, the blending structure is analogous to breaking down the large QDs in the embedding structure into smaller ones and then disperse them in the ZnS matrix. As such, with the blending structure the optical absorption should be stronger at short wavelength while weaker at long wavelength. This trend is revealed in Figure S4 in the Supporting Information, where the optical density below and above ~750 nm becomes higher and lower, respectively, for the blending with respect to the embedding architecture. The variation at long wavelength is not as obvious as that at the short wavelength region, because of relatively small absorption coefficient. The absorption edge at

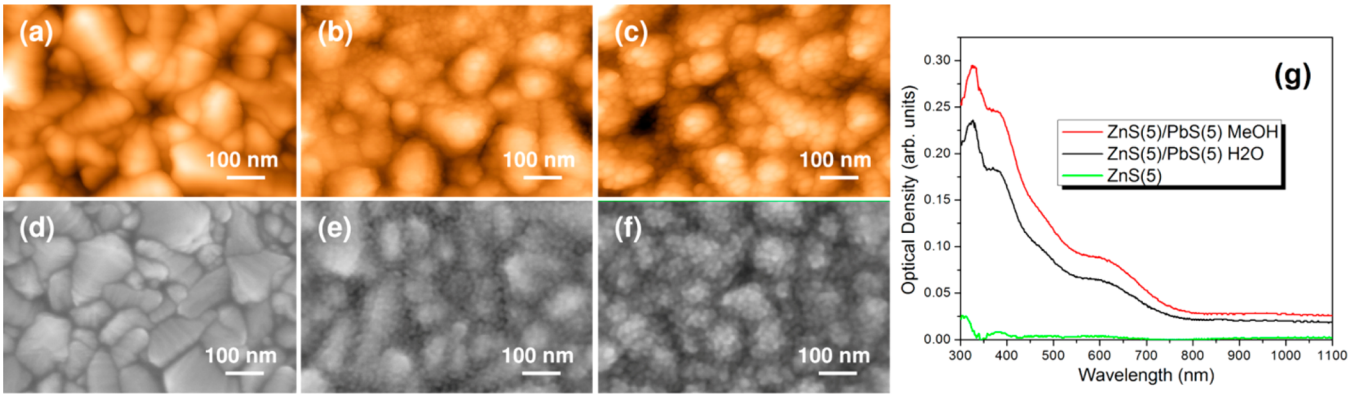

Figure 3. (a–c) AFM and (d–f) FESEM images of (a, d) bare FTO glass and ZnS(5)/PbS(5) films on FTO glasses prepared in (b, e) aqueous and (c, f) methanolic solutions. (g) Absorbance spectra of the corresponding ZnS(5)/PbS(5) films after subtracting the FTO portions. For comparison, the absorbance of ZnS(5) alone is also shown.

750 nm corresponds to a size of ~3 nm for PbS QDs.[33] This demonstrates that the increment in absorption at short wavelengths originates from QDs below 3 nm, consistent with the TEM images in Figure 1b and Figure S3 in the Supporting Information.

Growth of Overlayer. For photovoltaic application, an electron blocking layer is required to separate the TiO_2 substrate from touching the hole-collecting electrode. This can be realized by increasing the deposition round to form an overlayer. With both solvents, overlayers are produced on top of the bulk heterojunctions after filling up the mesoporous substrates, as shown in Figure S1 in the Supporting Information. The overlyer grows much faster in methanolic solution. It is estimated that the growth rate is approximately 100 nm per round of [PbS(5)/ZnS(5)] deposition in methanolic solution, whereas it is about 25 nm in aqueous solution. The PbS deposition rate can be computed by examining the contents of the relevant samples (EDS results from top surfaces of the samples in Figure S1 in the Supporting Information), i.e., Ti:Pb:Zn:S = 1:0.58:0.34:1.12 and 1:0.66:0.15:0.99 (in atomic ratio) for [PbS(5)/ZnS(5)]15 in methanol and [PbS(5)/ZnS(5)]20 in water, respectively. Considering the compositions of the bulk heterojunctions that presented above, the deposition rate of PbS is determined to be (0.58−0.23)/(15−5) = 0.035 (normalized to Ti content) per round in methanolic solution whereas (0.66−0.25)/(20−3) = 0.024 in aqueous solution. Therefore, methanol accelerates the formation of PbS in the overlayer.

Fabrication of PbS QDs by SILAR method resembles the ion association process in solution, i.e., Pb^{2+} ions are associated with S^{2-} ions (and/or HS^- ions; for clarity, only S^{2-} ions are mentioned below) to form PbS deposits. Two key factors affect the process: critical distance (q) and electrostatic force (F) between two ions of opposite charges. The critical distance determines the onset point for association to occur. If the distance between two ions (r) is smaller than q, the ions are associated; if $r > q$, they remain unassociated. The critical distance can be expressed as[30]

$$q = \frac{|z_+ z_-| N_A e^2}{8\pi\varepsilon_0\varepsilon_r RT} \quad (2)$$

where z_+ and z_- are the respective valence of cations and anions, N_A is the Avogadro constant, e is the elementary charge, ε_0 is the vacuum permittivity, ε_r is the relative permittivity (H_2O: 78.4, MeOH: 32.7, at 25 °C),[30] R is the gas constant, T is the absolute temperature. Accordingly, the critical distance in this study is determined to be about 1.4 and 3.4 nm in water and methanol, respectively. There is a minimum value of r, which equals to the sum of the radii of Pb^{2+} and S^{2-} ions or the half of the lattice constant of galena PbS, i.e., 0.3 nm. As such, an association region is established for each solvent, as illustrated in Figure 2b. Evidently, the region of methanol is nearly 3 times wider than that of water. To trigger the deposition, Pb^{2+} and S^{2-} ions have to be much closer to each other in water as compared to methanol (1.4 vs 3.4 nm). This indicates that ion association between Pb^{2+} and S^{2-} ions (or deposition of PbS) is much facilitated in methanol. The other factor of electrostatic interaction in the presence of solvent can be formulated as[30]

$$F = \frac{|z_+ z_-| e^2}{4\pi\varepsilon_0\varepsilon_r r^2} \quad (3)$$

The attractive forces between Pb^{2+} and S^{2-} ions are thus computed for different solvents, as presented in Figure 2b. It reveals that at the same distance the force in methanol is larger than water in light of the smaller ε_r, especially within the ion association region of water. This results in a larger driving force for the reaction. Hence, the deposition of PbS is much faster in methanol. In view of these, the smaller ε_r of methanol facilitates the ion association process through increasing the critical distance (thermodynamic factor) and enhancing the electrostatic force (kinetic factor), thereby accelerating the formation of PbS QDs in the overlayer where the spatial restrictions from the mesopores are absent.

To further verify the impact of solvent on overlayer growth, control experiments were carried out subsequently, where a single layer of ZnS(5)/PbS(5) film was deposited on a bare FTO glass substrate in either aqueous or methanolic solution. Figure 3a, d display the original surface morphology of the FTO substrate. Large particles of fluorine-doped tin oxide are clearly visible. After depositing a single layer of ZnS(5)/PbS(5) film with aqueous solution, minute quantum dots are formed on the FTO substrate, as shown in Figure 3b, e. The profile of the FTO particles is still discernible. In contrast, with the methanolic solution larger QDs are developed and deposited on the FTO substrate, making the profile of FTO particles blurred, as exhibited in Figure 3c, f. This indicates a fast growth of PbS quantum dots in methanolic solution, in accordance

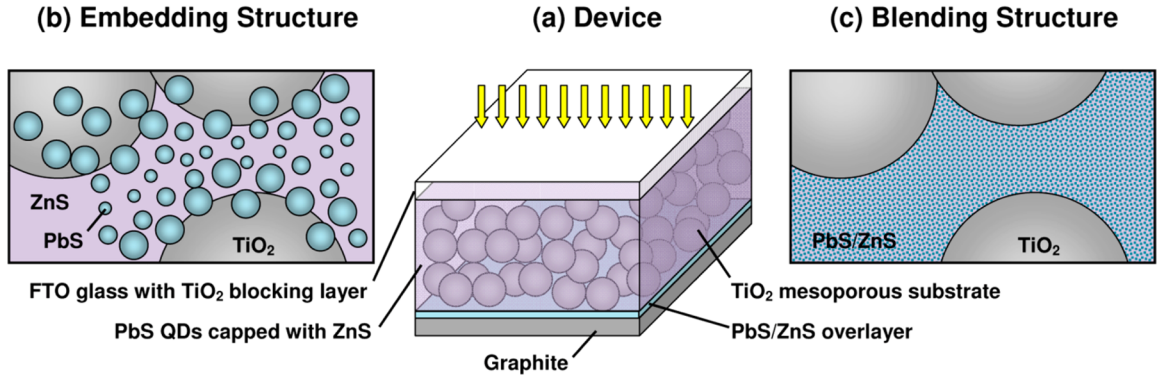

Figure 4. (a) Illustration of device structure with PbS quantum dots (b) embedded in and (c) blending with amorphous ZnS. Note that the size of quantum dots close to TiO_2 nanoparticles is generally larger than that away from the nanoparticles, as shown in Figure 1, which facilitates charge transport in view of the quantum confinement effect. The quantum dots on TiO_2 nanoparticles in a and c are not shown for clarity.

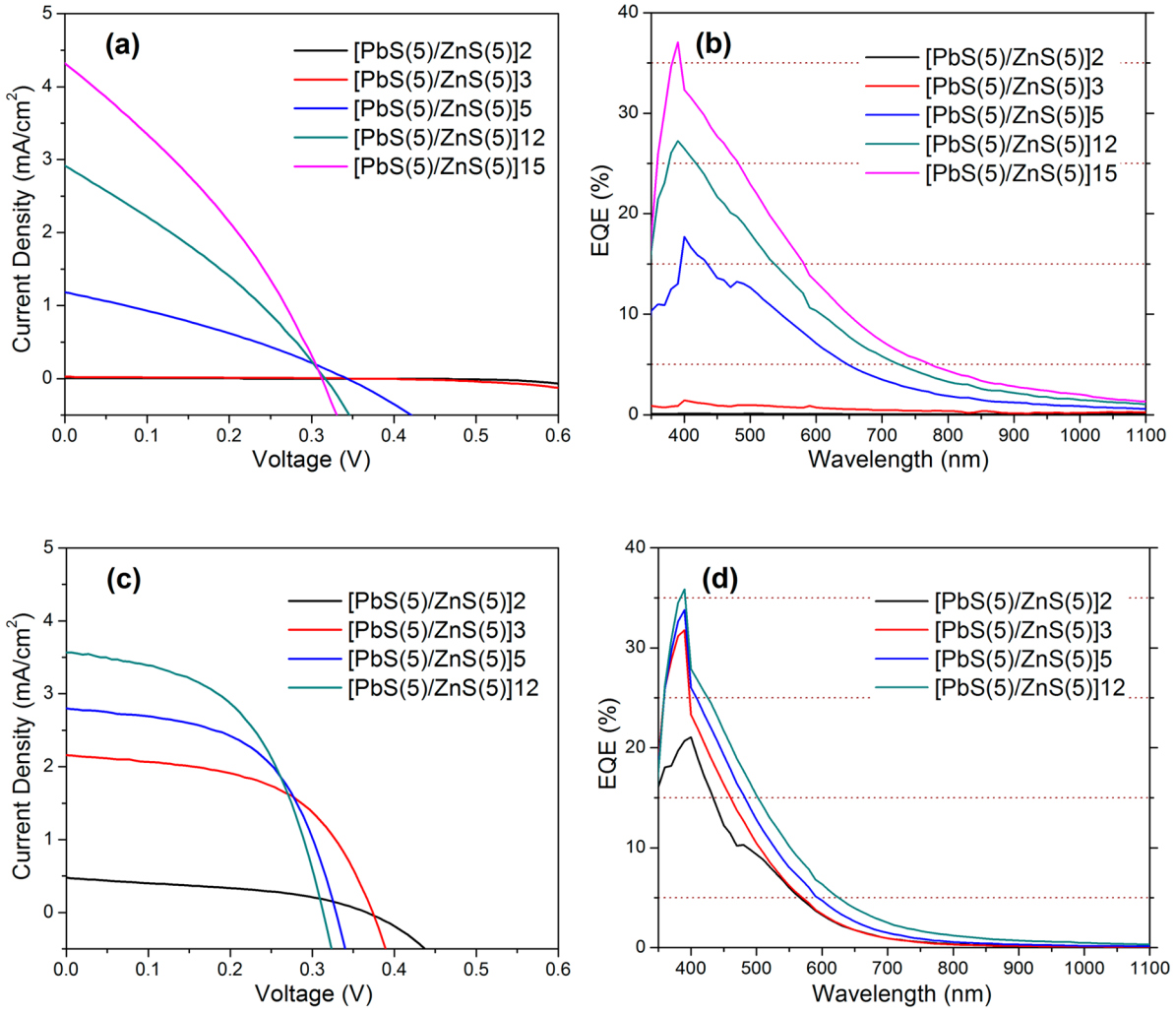

Figure 5. Photovoltaic performances of devices based on heterojunctions prepared in (a, b) methanolic and (c, d) aqueous solutions: (a, c) photocurrent–voltage characteristics and (b, d) external quantum efficiency.

with the above discussion. Corresponding absorbance spectra also discloses a stronger absorption of the ZnS(5)/PbS(5) film prepared in methanolic solution, in agreement with the film morphology, as shown in Figure 3g.

Photovoltaic Performance. Photovoltaic devices were assembled by employing graphite as the counter electrodes, as illustrated in Figure 4a. Upon illumination, incident photons are absorbed by the PbS QDs, generating excitons in the quantum dots. Direct injection of photogenerated electrons into the conduction band of *n*-type TiO_2 substrate takes place in the quantum dots directly contacting the substrate, provided that the QD size is below 7 nm,[34] which can be met for the QDs fabricated in this study. The QDs not contacting the substrate can transfer the electrons to the neighboring ones of

dx.doi.org/10.1021/am5035363 | ACS Appl. Mater. Interfaces 2014, 6, 14239–14246

comparable or larger size and eventually inject into the TiO_2 substrate. This is due to the fact that the QD size increases gradually when approaching the TiO_2 particles, as illustrated in Figure 4b and evidenced in Figure 1a and FigureS2a in the Supporting Information, yielding a favorable band alignment for charge transfer. The photogenerated holes are left transporting in the p-type PbS QDs. A better charge transport is anticipated with the blending structure in Figure 4(c), in light of the much small QDs and the very close distance between QDs. In this case, the driving force for charge injection is much increased due to smaller QD size. The transport of charge carriers would be facilitated, as the potential barrier imposed by ZnS becomes thinner and the barrier height is reduced considering the increased band gap energy of PbS. The overlayer not only segregates the TiO_2 substrate and the hole-collecting electrode, it also contributes to photocurrent through capturing additional photon energy. In this regard, a thick overlayer is preferred for sufficient light harvesting. However, this on the other hand increases charge transport distance especially for holes. Accordingly, there exists an optimal thickness of the overlayer to generate a compromise between light harvesting and charge collection. To this end, a series of experiments with different deposition rounds were performed to explore the best conditions. Figure 5a shows the photocurrent−voltage ($J-V$) characteristics of devices based on samples prepared in methanolic solution. In the first three rounds (i.e., n = 2 and 3), only very small photocurrent is generated, as a result of incomplete filling of the mesopores. No bulk heterojunctions are actually formed at this stage, thus resulting in very low photon-to-current response, as displayed in Figure 5b. Solar cells start functioning from five deposition rounds which are critical in filling up the mesopores and forming the bulk heterojunctions, as shown in Figure S1a in the Supporting Information. Photocurrent increases with the deposition round up to n = 15 at the expense of photovoltage. The $J-V$ curve at five rounds is ascribed to the performance of the bulk heterojunction alone (i.e., TiO_2 substrate filled with embedding structure). Therefore, the increment in photocurrent after five rounds originates from the formation of the overlayer, while the reduced photovoltage is due to increased recombination in thicker films. The contribution from the overlayer is appreciable. Figure 5c displays the $J-V$ curves of devices based on samples fabricated in aqueous solution. The solar cells begin to work at about only two rounds, and are fully functionalized after three rounds which are the critical point to create a bulk heterojunction as shown in Figure S1b in the Supporting Information. The photocurrent also increases with the deposition round but only up to n = 12, whereas the photovoltage decreases gradually. The photovoltaic performance at n = 3 is solely attributed to the bulk heterojunction itself (i.e., TiO_2 substrate filled with blending structure). The overlayer contributes less as compared to the one prepared in methanolic solution.

The bulk heterojunction alone shows superior performance for blending (n = 3, in water) with respect to embedding (n = 5, in methanol) structure. The higher photocurrent for the former comes from the higher EQE below 500 nm, above which the EQE becomes smaller (cf. Figure 5b, d). This is owing to the small crystallite size in the blending architecture, as shown in Figure 1. The EQE is in principle determined by light harvesting efficiency, charge separation efficiency, and charge collection efficiency. The light harvesting efficiency below 500 nm is almost unity for both heterojunctions based on the optical absorption in Figure S4 in the Supporting Information. As such, the charge separation and/or collection in this wavelength region should be more efficient with the blending configuration. This could be justified by the smaller crystallite size which yields better charge injection because of the quantum confinement effect, and by the shorter QD distance, which entails better charge transport, as illustrated in Figure 4b, c. However, in the wavelength region above 500 nm, the EQE is lower with the blending structure. This stems from the absence of large quantum dots in the bulk heterojunction.

In addition, it is noticed that the fill factor of the devices based on the blending structure is greatly larger than the embedding one, because of lower series resistance (R_s), as shown in Figure S5 in the Supporting Information. In the devices, all the components are kept the same except for the heterojunctions and the overlayers. This suggests that the PbS/ZnS structure itself affects the R_s considerably. The series resistance is extremely large with the incompletely filled heterojunctions (n < 3 for H_2O, n < 5 for MeOH), and drastically reduced by forming bulk heterojunctions (n = 3 for H_2O, n = 5 for MeOH), indicating that charge transport in the heterojunctions dominates the variation in resistance. Comparing the bulk heterojunctions alone, the series resistance of the blending configuration is about 5 times smaller than that of the embedding structure (see Figure S5 in the Supporting Information), suggesting that the charge transport be more efficient in the blending architecture. This is reasonable considering the very small distance between the QDs, as displayed in Figure 1b and Figure S3 in the Supporting Information, which facilitates charge transport process by forming minibands.[25] For further development of the encapsulating system, it might be useful to use other alternative matrix to replace the ZnS, provided that the requirements described above could be met. In this regard, CdS might be competent, which forms a similar type I heterojunction with PbS while providing a much smaller barrier height.[35,36]

CONCLUSION

Two distinct structures of bulk heterojunctions are produced by successive ionic layer adsorption and reaction through varying precursor solvent. With methanolic solution, spherical PbS quantum dots (QDs) of ∼5 nm embedded in the matrix of amorphous ZnS with substantial distance between the QDs are formed. In contrast, irregularly shaped PbS QDs of <3 nm blended with the amorphous ZnS with indiscernible spacing are constructed in aqueous solution. This can be attributed to a relatively low reactivity of Pb^{2+} ions in water, which impedes quantum dot growth. Overlayer also grows slower in aqueous solution (i.e., either overlayer thickness or PbS deposition rate), as a result of higher relative permittivity which gives rise to a smaller critical distance and driving force for PbS growth. The bulk heterojunction of the blending structure obtained in aqueous solution exhibits higher photovoltaic performance because of the small QD size and short distance between the QDs, and consequently more efficient charge injection and transport.

EXPERIMENTAL SECTION

Preparation and treatment of mesoporous TiO_2 substrates on FTO glasses followed the same procedures as our previous report.[17] The structure of PbS quantum dots embedded in ZnS matrix was obtained as follows. First, the PbS QDs were deposited by (1) dipping the substrates in 0.02 M $Pb(NO_3)_2$ methanolic solution for 30 s; (2)

rinsing with methanol for 1 min vigorously; (3) dipping in 0.02 M Na_2S dissolved in a mixture of methanol and water (v:v = 1:1) for 30 s; (4) rinsing with methanol for 1 min vigorously. These were repeated consecutively for 5 cycles in each PbS deposition run, i.e., PbS(5). Subsequently, the ZnS was deposited by (1) dipping the above samples in 0.1 M $Zn(CH_3COO)_2$ aqueous solution for 1 min; (2) rinsing with deionized water for 1 min vigorously; (3) dipping in 0.1 M Na_2S aqueous solution for 1 min; (4) rinsing with deionized water for 1 min vigorously. These were repeated successively for 5 cycles in each ZnS deposition run, i.e., ZnS(5). To fill up the mesoporous films and form overlayers, alternating deposition of the PbS(5) and ZnS(5) was carried out continuously, i.e., [PbS(5)/ZnS(5)]n with n being the deposition round. The architecture of PbS QDs blending with ZnS was prepared by replacing the solvent of methanol with water during PbS deposition, that is, (1) dipping in 0.02 M $Pb(NO_3)_2$ aqueous solution for 30 s; (2) rinsing with deionized water for 1 min vigorously; (3) dipping in 0.02 M Na_2S aqueous solution for 30 s; (4) rinsing with deionized water for 1 min vigorously. The procedures for the subsequent ZnS deposition were kept unchanged. For preparation of a single layer of ZnS(5)/PbS(5) on a bare FTO glass, all the precursors were the same as stated above, while the films were deposited by spin-assisted SILAR method at 2000 rpm for 1 min each cycle. All the deposition processes were carried out at ambient conditions. Photovoltaic devices were fabricated by employing the as-prepared samples as the working electrodes and graphite powders (<20 μm, Sigma-Aldrich) as the counter electrodes. The active area of devices was 0.20 cm^2.

Morphology of the QDs was examined with field emission transmission electron microscope (JEOL-JEM 2010F). Surface and cross-sectional views were characterized with field emission scanning electron microscope (ZEISS, SUPRA 40). Phase components were obtained by glancing angle X-ray diffractometer (PANalytical Empyrean, Cu Kα radiation). The J–V curves of the solar cells were measured using an AM 1.5 solar simulator (Newport, 300 W, calibrated with a Si reference cell) under a light intensity of 100 mW/cm^2. The EQE spectra were collected using a 300 W xenon lamp and a grating monochromator equipped with order sorting filters (Newport/Oriel). Absorption spectra were measured using a UV–vis–NIR spectrophotometer (Shimadzu, Solidspec-3700). Atomic force microscope (Bruker NanoScope) was also used to examine the morphology of the quantum dots on FTO substrates.

■ ASSOCIATED CONTENT

Supporting Information

FESEM cross-sectional views of bulk heterojunctions; low magnification TEM images of embending and blending structures; HRTEM image of blending structure; absorbance spectra of bulk heterojunctions; series resistance and fill factor as a function of deposition round. This material is available free of charge via the Internet at http://pubs.acs.org/.

■ AUTHOR INFORMATION

Corresponding Author

*E-mail: qing.wang@nus.edu.sg. Tel: +65 65167118. Fax: +65 67763604.

Notes

The authors declare no competing financial interest.

■ ACKNOWLEDGMENTS

This research is supported by the National Research Foundation Singapore under its Competitive Research Program (CRP Award NRF-CRP4-2008-03).

■ REFERENCES

(1) Green, M. A. Third Generation Photovoltaics: Ultra-high Conversion Efficiency at Low Cost. *Prog. Photovoltaics* **2001**, *9*, 123–135.

(2) Werner, J. H.; Brendel, R.; Queisser, H. J. Radiative Efficiency Limit of Terrestrial Solar Cells with Internal Carrier Multiplication. *Appl. Phys. Lett.* **1995**, *67*, 1028–1030.

(3) Hanna, M. C.; Nozik, A. J. Solar Conversion Efficiency of Photovoltaic and Photoelectrolysis Cells with Carrier Multiplication Absorbers. *J. Appl. Phys.* **2006**, *100*, 074510.

(4) Sukhovatkin, V.; Hinds, S.; Brzozowski, L.; Sargent, E. H. Colloidal Quantum-Dot Photodetectors Exploiting Multiexciton Generation. *Science* **2009**, *324*, 1542–1544.

(5) Sambur, J. B.; Novet, T.; Parkinson, B. A. Multiple Exciton Collection in a Sensitized Photovoltaic System. *Science* **2010**, *330*, 63–66.

(6) Semonin, O. E.; Luther, J. M.; Choi, S.; Chen, H.-Y.; Gao, J.; Nozik, A. J.; Beard, M. C. Peak External Photocurrent Quantum Efficiency Exceeding 100% via MEG in a Quantum Dot Solar Cell. *Science* **2011**, *334*, 1530–1533.

(7) Clifford, J. P.; Johnston, K. W.; Levina, L.; Sargent, E. H. Schottky Barriers to Colloidal Quantum Dot Films. *Appl. Phys. Lett.* **2007**, *91*, 253117.

(8) Luther, J. M.; Law, M.; Beard, M. C.; Song, Q.; Reese, M. O.; Ellingson, R. J.; Nozik, A. J. Schottky Solar Cells Based on Colloidal Nanocrystal Films. *Nano Lett.* **2008**, *8*, 3488–3492.

(9) Tang, J.; Brzozowski, L.; Barkhouse, D. A. R.; Wang, X.; Debnath, R.; Wolowiec, R.; Palmiano, E.; Levina, L.; Pattantyus-Abraham, A. G.; Jamakosmanovic, D.; Sargent, E. H. Quantum Dot Photovoltaics in the Extreme Quantum Confinement Regime: The Surface-Chemical Origins of Exceptional Air- and Light-Stability. *ACS Nano* **2010**, *4*, 869–878.

(10) Choi, J. J.; Lim, Y.-F.; Santiago-Berrios, M. B.; Oh, M.; Hyun, B.-R.; Sun, L.; Bartnik, A. C.; Goedhart, A.; Malliaras, G. G.; Abruna, H. D.; Wise, F. W.; Hanrath, T. PbSe Nanocrystal Excitonic Solar Cells. *Nano Lett.* **2009**, *9*, 3749–3755.

(11) Leschkies, K. S.; Beatty, T. J.; Kang, M. S.; Norris, D. J.; Aydil, E. S. Solar Cells Based on Junctions between Colloidal PbSe Nanocrystals and Thin ZnO Films. *ACS Nano* **2009**, *3*, 3638–3648.

(12) Pattantyus-Abraham, A. G.; Kramer, I. J.; Barkhouse, A. R.; Wang, X.; Konstantatos, G.; Debnath, R.; Levina, L.; Raabe, I.; Nazeeruddin, M. K.; Grätzel, M.; Sargent, E. H. Depleted-Heterojunction Colloidal Quantum Dot Solar Cells. *ACS Nano* **2010**, *4*, 3374–3380.

(13) Etgar, L.; Moehl, T.; Gabriel, S.; Hickey, S. G.; Eychmüller, A.; Grätzel, M. Light Energy Conversion by Mesoscopic PbS Quantum Dots/TiO_2 Heterojunction Solar Cells. *ACS Nano* **2012**, *6*, 3092–3099.

(14) Barkhouse, D. A. R.; Debnath, R.; Kramer, I. J.; Zhitomirsky, D.; Pattantyus-Abraham, A. G.; Levina, L.; Etgar, L.; Grätzel, M.; Sargent, E. H. Depleted Bulk Heterojunction Colloidal Quantum Dot Photovoltaics. *Adv. Mater.* **2011**, *23*, 3134–3138.

(15) Kramer, I. J.; Zhitomirsky, D.; Bass, J. D.; Rice, P. M.; Topuria, T.; Krupp, L.; Thon, S. M.; Ip, A. H.; Debnath, R.; Kim, H.-C.; Sargent, E. H. Ordered Nanopillar Structured Electrodes for Depleted Bulk Heterojunction Colloidal Quantum Dot Solar Cells. *Adv. Mater.* **2012**, *24*, 2315–2319.

(16) Lan, X.; Bai, J.; Masala, S.; Thon, S. M.; Ren, Y.; Kramer, I. J.; Hoogland, S.; Simchi, A.; Koleilat, G. I.; Paz-Soldan, D.; Ning, Z.; Labelle, A. J.; Kim, J. Y.; Jabbour, G.; Sargent, E. H. Self-Assembled, Nanowire Network Electrodes for Depleted Bulk Heterojunction Solar Cells. *Adv. Mater.* **2013**, *25*, 1769–1773.

(17) Sun, L.; Koh, Z. Y.; Wang, Q. PbS Quantum Dots Embedded in a ZnS Dielectric Matrix for Bulk Heterojunction Solar Cell Applications. *Adv. Mater.* **2013**, *25*, 4598–4604.

(18) Leventis, H. C.; O'Mahony, F.; Akhtar, J.; Afzaal, M.; O'Brien, P.; Haque, S. A. Transient Optical Studies of Interfacial Charge Transfer at Nanostructured Metal Oxide/PbS Quantum Dot/Organic Hole Conductor Heterojunctions. *J. Am. Chem. Soc.* **2010**, *132*, 2743–2750.

(19) Patel, A. A.; Wu, F.; Zhang, J. Z.; Torres-Martinez, C. L.; Mehra, R. K.; Yang, Y.; Risbud, S. H. Synthesis, Optical Spectroscopy and

Ultrafast Electron Dynamics of PbS Nanoparticles with Different Surface Capping. *J. Phys. Chem. B* **2000**, *104*, 11598−11605.
(20) Tang, J.; Kemp, K. W.; Hoogland, S.; Jeong, K. S.; Liu, H.; Levina, L.; Furukawa, M.; Wang, X.; Debnath, R.; Cha, D.; Chou, K. W.; Fischer, A.; Amassian, A.; Asbury, J. B.; Sargent, E. H. Colloidal-Quantum-Dot Photovoltaics Using Atomic-Ligand Passivation. *Nat. Mater.* **2011**, *10*, 765−771.
(21) Ip, A. H.; Thon, S. M.; Hoogland, S.; Voznyy, O.; Zhitomirsky, D.; Debnath, R.; Levina, L.; Rollny, L. R.; Carey, G. H.; Fischer, A.; Kemp, K. W.; Kramer, I. J.; Ning, Z.; Labelle, A. J.; Chou, K. W.; Amassian, A.; Sargent, E. H. Hybrid Passivated Colloidal Quantum Dot Solids. *Nat. Nanotechnol.* **2012**, *7*, 577−582.
(22) Kovalenko, M. V.; Scheele, M.; Talapin, D. V. Colloidal Nanocrystals with Molecular Metal Chalcogenide Surface Ligands. *Science* **2009**, *324*, 1417−1420.
(23) Lee, J.-S.; Kovalenko, M. V.; Huang, J.; Chung, D. S.; Talapin, D. V. Band-like Transport, High Electron Mobility and High Photoconductivity in All-Inorganic Nanocrystal Arrays. *Nat. Nanotechnol.* **2011**, *6*, 348−352.
(24) Tsokkou, D.; Papagiorgis, P.; Protesescu, L.; Kovalenko, M. V.; Choulis, S. A.; Christofides, C.; Itskos, G.; Othonos, A. Photophysics of PbS Quantum Dot Films Capped with Arsenic Sulfide Ligands. *Adv. Energy Mater.* **2014**, *4*, 1301547.
(25) Nozik, A. J. Spectroscopy and Hot Electron Relaxation Dynamics in Semiconductor Quantum Wells and Quantum Dots. *Annu. Rev. Phys. Chem.* **2001**, *52*, 193−231.
(26) Jeong, K. S.; Tang, J.; Liu, H.; Kim, J.; Schaefer, A. W.; Kemp, K.; Levina, L.; Wang, X.; Hoogland, S.; Debnath, R.; Brzozowski, L.; Sargent, E. H.; Asbury, J. B. Enhanced Mobility-Lifetime Products in PbS Colloidal Quantum Dot Photovoltaics. *ACS Nano* **2012**, *6*, 89−99.
(27) Gao, Y.; Aerts, M.; Sandeep, C. S. S.; Talgorn, E.; Savenije, T. J.; Kinge, S.; Siebbeles, L. D. A.; Houtepen, A. J. Photoconductivity of PbSe Quantum-Dot Solids: Dependence on Ligand Anchor Group and Length. *ACS Nano* **2012**, *6*, 9606−9614.
(28) Law, M.; Luther, J. M.; Song, Q.; Hughes, B. K.; Perkins, C. L.; Nozik, A. J. Structural, Optical, and Electrical Properties of PbSe Nanocrystal Solids Treated Thermally or with Simple Amines. *J. Am. Chem. Soc.* **2008**, *130*, 5974−5985.
(29) Luther, J. M.; Law, M.; Song, Q.; Perkins, C. L.; Beard, M. C.; Nozik, A. J. Structural, Optical, and Electrical Properties of Self-Assembled Films of PbSe Nanocrystals Treated with 1,2-Ethanedithiol. *ACS Nano* **2008**, *2*, 271−280.
(30) Izutsu, K. *Electrochemistry in Nonaqueous Solutions*; Wiley−VCH: Weinheim, Germany, 2002.
(31) Kalidas, C.; Hefter, G.; Marcus, Y. Gibbs Energies of Transfer of Cations from Water to Mixed Aqueous Organic Solvents. *Chem. Rev.* **2000**, *100*, 819−852.
(32) Joo, J.; Na, H. B.; Yu, T.; Yu, J. H.; Kim, Y. W.; Wu, F.; Zhang, J. Z.; Hyeon, T. Generalized and Facile Synthesis of Semiconducting Metal Sulfide Nanocrystals. *J. Am. Chem. Soc.* **2003**, *125*, 11100−11105.
(33) Hyun, B.-R.; Zhong, Y.-W.; Bartnik, A. C.; Sun, L.; Abruna, H. D.; Wise, F. W.; Goodreau, J. D.; Matthews, J. R.; Leslie, T. M.; Borrelli, N. F. Electron Injection from Colloidal PbS Quantum Dots into Titanium Dioxide Nanoparticles. *ACS Nano* **2008**, *2*, 2206−2212.
(34) Acharya, K. P.; Hewa-Kasakarage, N. N.; Alabi, T. R.; Nemitz, I.; Khon, E.; Ullrich, B.; Anzenbacher, P.; Zamkov, M. Synthesis of PbS/TiO_2 Colloidal Heterostructures for Photovoltaic Applications. *J. Phys. Chem. C* **2010**, *114*, 12496−12504.
(35) Kinder, E.; Moroz, P.; Diederich, G.; Johnson, A.; Kirsanova, M.; Nemchinov, A.; O'Connor, T.; Roth, D.; Zamkov, M. Fabrication of All-Inorganic Nanocrystal Solids through Matrix Encapsulation of Nanocrystal Arrays. *J. Am. Chem. Soc.* **2011**, *133*, 20488−20499.
(36) Moroz, P.; Kholmicheva, N.; Mellott, B.; Liyanage, G.; Rijal, U.; Bastola, E.; Huband, K.; Khon, E.; McBride, K.; Zamkov, M. Suppressed Carrier Scattering in CdS-Encapsulated PbS Nanocrystal Films. *ACS Nano* **2013**, *7*, 6964−6977.